Comput Mech (2007) 40:837–853
DOI 10.1007/s00466-006-0145-7

ORIGINAL PAPER

A regularized least-squares radial point collocation method (RLS-RPCM) for adaptive analysis

Bernard B. T. Kee · G. R. Liu · C. Lu

Received: 11 May 2006 / Accepted: 4 November 2006 / Published online: 29 November 2006

Abstract This paper presents a stabilized meshfree method formulated based on the strong formulation and local approximation using radial basis functions (RBFs). The purpose of this paper is two folds. First, a regularization procedure is developed for stabilizing the solution of the radial point collocation method (RPCM). Second, an adaptive scheme using the stabilized RPCM and residual based error indicator is established. It has been shown in this paper that the features of the meshfree strong-form method can facilitated an easier implementation of adaptive analysis. A new error indicator based on the residual is devised and used in this work. As shown in the numerical examples, the new error indicator can reflect the quality of the local approximation and the global accuracy of the solution. A number of examples have been presented to demonstrate the effectiveness of the present method for adaptive analysis.

Keywords Meshfree method · Strong-form formulation · Radial basis function · Adaptive analysis · Delaunay diagram · Error indicator · Regularization technique

B. B. T. Kee (✉) · G. R. Liu
Centre for Advanced Computations in Engineering Science (ACES), Department of Mechanical Engineering, National University of Singapore, 9 Engineering Drive 1, Singapore 117576, Singapore
e-mail: g0301110@nus.edu.sg

G. R. Liu
The Singapore-MIT Alliance (SMA), E4-04-10, 4 Engineering Drive 3, Singapore 117576, Singapore
e-mail: mpeliugr@nus.edu.sg

C. Lu
Institute of High Performance Computing (IHPC), 1 Science Park II, Singapore 117528, Singapore
e-mail: luchun@ihpc.a-star.edu.sg

1 Introduction

Undoubtedly, finite element method (FEM) is one of the most successful numerical methods invented in the last century. FEM has been developed since 1950 and achieved remarkable progress in various fields. However, the inherited shortcoming of FEM has also been revealed along the progress of development. In the formulation of FEM, the continuous problem domain is discretized into many meshes. Due to the use of mesh, FEM encounters difficulty while dealing with those problems which involve in high distortion, large deformation, explosion, crack propagation etc.

Since the main drawback of FEM is caused by the used of mesh, it motivates and leads to the development of a new generation of numerical method, meshfree method, which is formulated without relying on mesh. Such salient feature has been drawing many attentions and gaining great interest in the computational mechanics community in the past few decades. Hence, many meshfree methods has been proposed and developed. Intensive reviews of various meshfree methods and their development are abundantly available in literature [3,14,18].

Meshfree methods can be classified into three major categories according to their formulation procedure. The majority of the existing meshfree methods are formulated based on the weak formulation, or short for meshfree weak-form method. Element-free Galerkin (EFG) method [2], meshless local Petrov-Galerkin (MLPG) method [1], local radial point interpolation method (LRPIM) [16], the point interpolation method [15,25,34] and reproducing kernel particle method (RKPM) [10,20] are under the categories of meshfree weak-form method. The meshfree weak-form methods do not

require mesh for function approximation but background mesh is still needed for integration resultant from the used of weak formulation, and hence is not regarded as "truly" mesh free. The second category of meshfree method is formulated based on strong formulation, or short for meshfree strong-form method, including finite point method [29], radial point collocation method [26], smooth hydrodynamics method [22,27] etc. The meshfree strong-form method does not use mesh for both field function approximation and background integration, and therefore it is regarded as a "truly" meshfree method. The last category of meshfree method is formulated based on both weak and strong formulation, for instance, the meshfree weak-strong forms (MWS) method [23]. The weak-strong form method requires mesh for derivative boundary. A more detailed reviews on these methods can be found in the book by Liu and Gu [14,18].

Function approximation based on the scattered nodes is the key ingredient in the meshfree method. Moving least-square (MLS) approximation [2,28], integral form of approximation i.e. RKPM [10,20] and point interpolation approximation are commonly used in the meshfree method. In this paper, point interpolation approximation is adopted and based on the radial basis function and polynomial function using local nodes. The idea of using RBFs globally for solving PDEs was introduced by Kansa [11]. Since then many of the research woks have been carried out extensively [5,6,9,12,30,35]. However, the global RBF scheme results in a full coefficient matrix incurs high computational cost and also leads to ill condition [12]. In the recent years, a series of meshfree method which formulated based on local nodes has been actively discussed and well studied [13,16,17,23,24,34], including the radial point collocation method (RPCM) [26].

Besides using local RBF scheme, the most distinguish feature of the RLS-RPCM is that it is formulated based on strong formulation. In our work, we regards RLS-RPCM as a truly mesh free method as, (1) no mesh is needed for constructing shape functions, and (2) no background mesh is needed in the present formulation. Hence, the formulation procedure is simple and straight forward, integration is not required in the formulation procedure which makes it a good candidate for adaptive analysis. However, due to the use of the local nodes, unstable solution is often obtained when Neumann boundary condition exists, which limits its application for the practical problems that often require adaptive analysis. Without an effective stabilization measure, it is impossible to use the RPCM for adaptive analysis. This argument will be clearly demonstrated in the numerical examples.

The purpose of this paper is therefore, at first, to develop a regularization procedure for stabilizing the solution of the RPCM. Secondly, an adaptive scheme using stabilized RPCM and residual based error indicator is established.

Regularization technique is commonly used for stabilizing the solution of ill-posed inverse problem [19]. It is employed to restore the stability of the RPCM solution for the forward problem in this work. After the stability is restored, the attractive features of the strong-form meshfree method can then be utilized to facilitate an easier implementation of adaptive analysis. In the adaptive procedure, a reliable and effective error indicator plays a very crucial role. A residual based error indicator is proposed and used in this work. A number of numerical examples has shown that the error indicator is simple and well reflects the quality of the local approximation and the global accuracy of the solution.

A simple nodal refinement scheme based on the Delaunay diagram is employed in this work. As the RPCM is regarded as a truly meshfree method, node insertions can be easily implemented without worry about the nodal connectivity. With all these key ingredients of techniques: stabilization, error estimation and nodal refinement, the stabilized RPCM can perform adaptive analysis effectively to obtain solutions with desired accuracy automatically as shown in the numerical examples.

2 Function approximation

The radial basis functions (RBFs) have been widely used for function approximation in the mathematic community [4,8]. In early 1990s, Kansa had used RBFs for solving partial differential equations (PDEs) [11]. In his works, all nodes in the problem domain are used for the function approximation, the full coefficient matrix not only incurs large computation and also large condition number [12]. In contrast to Kansa's works, our function approximation is constructed locally, only vicinity nodes are involved for the local approximation. There are many RBFs available in the literature. Typical generalized RBFs with arbitrary real shape parameters [14,18] are listed in the Table 1.

Consider an unknown field function $u(\mathbf{x})$ can be approximated at an interest point $\mathbf{x}$ in the problem domain by radial point interpolation in the following form:

$$u^h(\mathbf{x}) = \sum_{i=1}^{n} a_i r_i(\|\mathbf{x} - \mathbf{x}_i\|) + \sum_{j=1}^{m} b_j p_j, \tag{1}$$

where n is the total number of the supporting nodes in the local domain, m is the number of monomials in the

Table 1 Typical generalized radial basis functions [14,18], where $r_i = \|\mathbf{x} - \mathbf{x}_i\|$ is the Euclidian norm in the vector space

Type	Expression	Dimensionless parameter
Multi-quadrics (MQ)	$R_i(x,y) = \left(r_i^2 + (\alpha_c d_c)^2\right)^q$	α_c, q
Gaussian (EXP)	$R_i(x,y) = \exp\left(-c r_i^2\right)$	c
Thin plate spline (TPS)	$R_i(x,y) = r_i^\eta$	η
Logarithmic	$R_i(x,y) = r_i^\eta \log r_i$	η

polynomial function, $r_i(\|\cdot\|)$ is the radial basis function and p_j is the monomial in polynomial function for augmentation. a_i and b_j are the coefficient of radial basis function and monomial of polynomial function.

By enforcing the interpolation passing through the nodal values at the nodes, the following expression can be obtained,

$$\begin{bmatrix} u_1 \\ u_2 \\ \vdots \\ u_n \end{bmatrix} = \begin{bmatrix} r_1(\|\mathbf{x}_1 - \mathbf{x}_1\|) & r_1(\|\mathbf{x}_1 - \mathbf{x}_2\|) & \cdots & r_1(\|\mathbf{x}_1 - \mathbf{x}_n\|) & p_1(\mathbf{x}_1) & \cdots & p_m(\mathbf{x}_1) \\ r_2(\|\mathbf{x}_2 - \mathbf{x}_1\|) & r_2(\|\mathbf{x}_2 - \mathbf{x}_2\|) & \cdots & r_2(\|\mathbf{x}_2 - \mathbf{x}_n\|) & p_1(\mathbf{x}_2) & \cdots & p_m(\mathbf{x}_2) \\ \vdots & \vdots & \ddots & \vdots & \vdots & \ddots & \vdots \\ r_n(\|\mathbf{x}_n - \mathbf{x}_1\|) & r_n(\|\mathbf{x}_n - \mathbf{x}_2\|) & \cdots & r_n(\|\mathbf{x}_n - \mathbf{x}_n\|) & p_1(\mathbf{x}_n) & \cdots & p_m(\mathbf{x}_n) \end{bmatrix} \begin{bmatrix} a_1 \\ \vdots \\ a_n \\ b_1 \\ \vdots \\ b_m \end{bmatrix}$$

or

$$\mathbf{U} = \begin{bmatrix} \mathbf{R} & \mathbf{P} \end{bmatrix} \begin{bmatrix} \mathbf{a} \\ \mathbf{b} \end{bmatrix}, \tag{2}$$

where $\mathbf{U}$ is the vector of unknown nodal values, $\mathbf{a}$ and $\mathbf{b}$ are the vector of coefficients of radial basis functions and monomials of the polynomial function, respectively.

With the orthogonal condition [8,12],

$$\mathbf{P}^{\mathrm{T}}\mathbf{a} = 0, \tag{3}$$

the vector of coefficients can be obtained as

$$\begin{bmatrix} \mathbf{a} \\ \mathbf{b} \end{bmatrix} = \begin{bmatrix} \mathbf{R} & \mathbf{P} \\ \mathbf{P}^{\mathrm{T}} & 0 \end{bmatrix}^{-1} \begin{Bmatrix} \mathbf{U} \\ 0 \end{Bmatrix} = \mathbf{G}^{-1} \begin{Bmatrix} \mathbf{U} \\ 0 \end{Bmatrix}. \tag{4}$$

Therefore, the approximated unknown field function $u(\mathbf{x})$ at interest point $\mathbf{x}$ can be expressed as

$$u^h(\mathbf{x}) = \begin{bmatrix} \phi_1(\mathbf{x}) & \phi_2(\mathbf{x}) & \cdots & \phi_n(\mathbf{x}) \end{bmatrix} \mathbf{U} = \Phi(\mathbf{x})\mathbf{U}, \tag{5}$$

where $\phi(\mathbf{x})$ is the shape function called RPIM shape function.

The derivative of the field function can be easily obtained through differentiating the shape functions. For example, the first derivative of the field function with respect to k can be expressed as

$$u^h_{,k}(\mathbf{x}) = \Phi_{,k}(\mathbf{x})\mathbf{U}. \tag{6}$$

The details of constructing the RPIM shape function can be found in e.g., [14,18].

One important property of the above shape function shown in Eq. (5) is that RPIM shape function possesses Kronecker delta property. Without special treatment, other function approximations like MLS approximation and reproducing kernel particle approximation do not possesses Kronecker delta property. Imposition of essential boundary condition could be an issue to be resolved. Since the RPIM shape functions process Kronecker delta property, the essential boundary conditions can be directly imposed without any special treatment. More properties of RPIM shape function is revealed and well discussed in the [14,18].

In this work, multiquadrics (MQ) and completed second order polynomial are used in the function approximation. The shape parameters used for MQ is adopted from the recommended values reported by Liu et al. [14,18,33]: $\alpha_c = 3.0$ and $q = 1.03$.

2.1 Nodal selection

To construct RPIM shape function, polynomial function augmented with RBF is used in the approximation function. To solve the vector of coefficients in Eq. (4), the number of supporting node, n, can not be less the number of monomial terms, m, in the polynomial function.

$$n >> m \tag{7}$$

Besides, to avoid rank deficiency in the stiffness matrix, we should not solely select the supporting node based on their physical distance to collocation point. The supporting nodes must at least form a "layer" of nodes to surround the collocation point. For instance, in the case of one dimension, the nodes on the left and right hand side of the collocation point must be included as the supporting nodes, as shown in Fig. 1.

For regularly distributed nodes in two-dimensional case, the number of supporting could be nine nodes which is the optimal number of forming one "layer" of nodes to surround the collocation point. Two to three times of the number of monomial terms is the suggested number of nodes for constructing RPIM in the domain with irregularly distributed nodes (see Fig. 2).

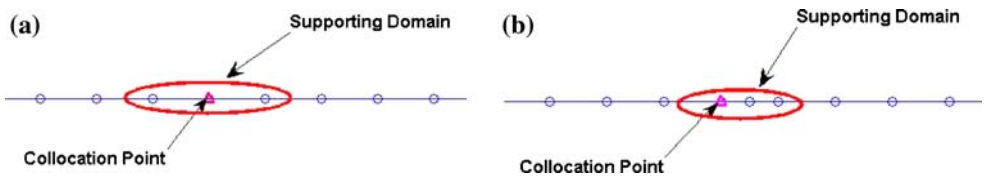

Fig. 1 **a** Appropriate nodal selection, **b** inappropriate nodal selection in one dimension problem domain

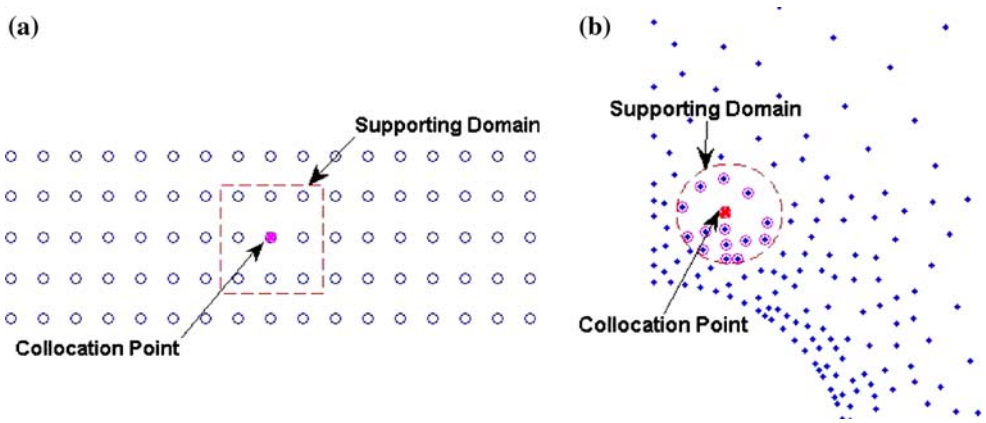

Fig. 2 Nodal selection for **a** regular and **b** irregular node distribution in two dimension problem domain

3 Radial point collocation method

Consider a problem in a domain is governed by the following PDEs:

$$L(u) = f \quad \text{in } \Omega, \tag{8}$$

with Neumann boundary conditions

$$B(u) = g \quad \text{on } \Gamma_{\mathrm{t}}, \tag{9}$$

and Dirichlet boundary conditions

$$u = \bar{u} \quad \text{on } \Gamma_{\mathrm{u}}, \tag{10}$$

where $L(), B()$ are the differential operators and u is the field variable.

Assume that the above equations, Eqs. (8)–(10), can be collocated at the field nodes in the problem domain and on the boundaries, respectively, the discretized governing system equations can be shown as follows.

$$L(u_i) = f_i \quad \text{in } \Omega, \tag{11}$$

with Neumann boundary conditions

$$B(u_i) = g_i \quad \text{on } \Gamma_{\mathrm{t}}, \tag{12}$$

and Dirichlet boundary conditions

$$u_i = \bar{u}_i \quad \text{on } \Gamma_{\mathrm{u}}, \tag{13}$$

where subscript "i" denotes the collocation point.

The governing system equations, Eqs. (11)–(14), can be collocated at their corresponding field nodes then be assembled and expressed in the following matrix form as

$$\mathbf{KU} = \mathbf{F}, \tag{14}$$

where $\mathbf{K}$ is the stiffness matrix, $\mathbf{F}$ is the force vector and $\mathbf{U}$ is the vector of unknown nodal values. Note that the stiffness matrix of the collocation method is generally unsymmetric.

The vector of unknown nodal values can be easily solved as

$$\mathbf{U} = \mathbf{K}^{-1}\mathbf{F}, \tag{15}$$

if $\mathbf{K}$ is not singular and well-conditioned.

4 Regularization procedure

Regularization technique is a very common technique used for stabilizing the solutions of the ill-posed inverse problems [19]. In this paper, instead of using the regularization technique for inverse problems, this technique is employed to stabilize the solutions of the RPCM for the forward problems. In our regularization procedure, Tikhonov regularization technique [19,31] is adopted. By making use of the governing system equations as a priori information, the regularization matrix and vector

are formed. The regularization procedure is briefed as follows.

4.1 Regularization equations

To form the regularization matrix and vector, priori information is required. In the present formulation, the governing system equations, Eqs. (8)–(10), are used as the regularization equations for constructing the regularization matrix and vector.

Consider a problem governed by a set of PDEs as given in Eqs. (8)–(10), and the PDEs can be used as the regularization equations. The regularization equations can be collocated at the regularization points respectively as shown in Fig. 3. Therefore, we have

$$L(u_r) = f_r \quad \text{in } \Omega, \tag{16}$$

with Neumann boundary conditions

$$B(u_r) = g_r \quad \text{on } \Gamma_t, \tag{17}$$

and Dirichlet boundary conditions

$$u_r = \bar{u}_r \quad \text{on } \Gamma_u, \tag{18}$$

where subscript "r" denotes the regularization point.

The regularization points in the internal problem domain are same as the interior field nodes. Else, the regularization points along the boundaries are allocated in between the boundary nodes as shown in Fig. 3.

After collocating the regularization equations at their respective regularization points, a set of resultant algebraic equations can be formed and expressed as the following matrix form as

$$\mathbf{K}_r\mathbf{U} = \mathbf{F}_r, \tag{19}$$

where $\mathbf{K}_r$ is the regularization matrix and $\mathbf{F}_r$ is the regularization vector. Note that the total number of algebraic equations is same as the total number of the unknown nodal values in the problem domain.

4.2 Regularization least-squares formulation

First, we define a functional Π as follows [19],

$$\Pi = \{\mathbf{KU} - \mathbf{F}\}^{\mathrm{T}}\{\mathbf{KU} - \mathbf{F}\} + \alpha\{\mathbf{K}_r\mathbf{U} - \mathbf{F}_r\}^{\mathrm{T}}\{\mathbf{K}_r\mathbf{U} - \mathbf{F}_r\}, \tag{20}$$

where α is the regularization factor which determine the degree of regularization. The first term of Eq. (20) is the L_2 norm of the residual of the governing equations, and the second term is the L_2 norm of the residual of the regularization equations. Hence, functional Π is the total sum of the both residuals in the system.

Seek for the minimal Π with respect to the unknown vector $\mathbf{U}$, the following equation can be obtained.

$$\frac{\partial \Pi}{\partial \mathbf{U}} = 2\mathbf{K}^{\mathrm{T}}\{\mathbf{KU} - \mathbf{F}\} + 2\alpha\mathbf{K}_r^{\mathrm{T}}\{\mathbf{K}_r\mathbf{U} - \mathbf{F}_r\} = 0. \tag{21}$$

The above equation can be rearranged and leads to the following equation,

$$\left[\mathbf{K}^{\mathrm{T}}\mathbf{K} + \alpha\mathbf{K}_r^{\mathrm{T}}\mathbf{K}_r\right]\mathbf{U} = \mathbf{K}^{\mathrm{T}}\mathbf{F} + \alpha\mathbf{K}_r^{\mathrm{T}}\mathbf{F}_r$$

or

$$\hat{\mathbf{K}}\mathbf{U} = \hat{\mathbf{F}}, \tag{22}$$

where $\hat{\mathbf{K}}$ is the regularized coefficient matrix and $\hat{\mathbf{F}}$ is the regularized force vector.

The vector of unknown nodal values can be solved as

$$\mathbf{U} = \hat{\mathbf{K}}^{-1}\hat{\mathbf{F}}, \tag{23}$$

if $\hat{\mathbf{K}}$ is invertible and well-conditioned.

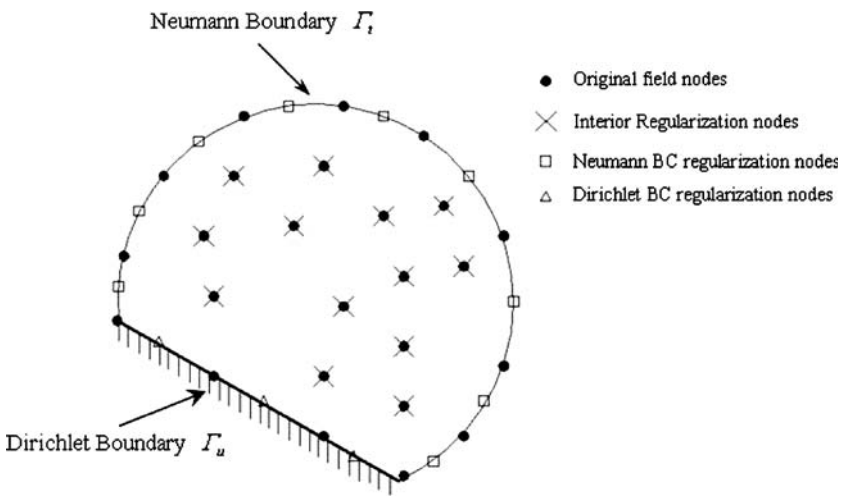

Fig. 3 Regularization points in a problem domain and boundaries

The drawback of the regularization procedure is that the condition number of the regularized coefficient matrix $\hat{\mathbf{K}}$ is much larger than the stiffness matrix $\mathbf{K}$. However, one can notice in Eq. (22) that $\hat{\mathbf{K}}$ is a symmetric and positive definite (SPD) matrix. With the SPD property, the linear solver like Cholesky solver can be used to solve for the solution more accurately and efficiently. The computational error caused by large condition number can also be reduced.

4.3 Determination of regularization factor

From Eq. (22) one can observe that the regularization factor α directly affects the regularized coefficient matrix and force vector. The degree of regularization solely depends on the values of regularization factor, hence the determination of an appropriate regularization factor is very crucial. The value of regularization factor, α, should be positive and ranged from zero to infinity. When $\alpha = 0$, the effect of regularization is vanished. The RLS-RPCM is reduced to the original RPCM. If α is equal to infinity, the effect of regularization is also vanished as the solution is solely based on the Eq. (19). Both solutions are unstable. The appropriate α should provide a minimum residual for both terms in Eq. (20) [7,21].

From our previous work [21], the governing equation, Eq. (11), is used for constructing the regularization matrix for the regularization points along the boundary only. With such regularization scheme, L-curve approach [7] was required to determine an appropriate regularization factor. The determination process could be tedious and an additional computational cost was incurred.

However, due to the special regularization equations and regularization points used in our scheme, the determination of regularization factor can be avoided. The vector of unknown nodal values $\mathbf{U}$ can be solved either by Eq. (14) or Eq. (19), however, none of the solutions is stable. By solving the same status problem with two differences sets of discretized equations, the regularization procedure provide a compromise solution to satisfied both sets of system equations with minimum residual. Hence, $\alpha = 1$ is a logical choice to be used in our formulation.

5 Adaptive scheme

As the radial point collocation method (RPCM) is a truly meshfree method, it possess attractive features to facilitate an easier implementation of adaptive scheme. Without the constraint of the nodal connectivity, additional nodes can be inserted during refinement process easily.

A good error indicator is very important in the adaptive analysis. In this paper, an error indicator based on residual of the system governing equations is proposed. The residual based error indicator provides a good measurement for the quality of the local approximation and the global accuracy of the solution. The details of the error indicator and refinement procedures are given as follows.

5.1 Error indicator

The new error indicator is devised based on the residual of the governing equations. In the strong-form collocation method, the governing equations are fully satisfied at the interior nodes, but not elsewhere. In our adaptive scheme, the problem domain is first represented using Delaunay diagram. The residual of the governing equations is then measured at the center of the Delaunay cells. The error indicator indicates the error over a local region and it is defined as follows:

$$\eta_j = \frac{1}{3} A_j \left\| Lu_j - f_j \right\|_{L_2}, \tag{24}$$

where A_j is the area of the jth Delaunay cell and the $\left\| Lu_j - f_j \right\|_{L_2}$ is the L_2 norm of the residual of the governing equation measured at the center of the corresponding cell.

With the above definition of the local error indicator, the estimated global residual norm can be easily obtained by integrating the residual over the entire domain

$$\begin{aligned} \eta_g &= \int_{\Omega} \eta \mathrm{d}\Omega \\ &= \sum_{j=1}^{\mathrm{nc}} \frac{1}{3} A_j \left\| Lu_j - f_j \right\|_{L_2}, \end{aligned} \tag{25}$$

where nc is the total number of Delaunay cells.

5.2 Refinement and stopping criteria

Node is inserted at the center of the cell if the following refinement criteria is met.

$$\eta_j \geq \kappa_l \eta_m, \tag{26}$$

where κ_l is the local refinement coefficient and

$$\eta_m = \max\left(\eta_j\right). \tag{27}$$

The estimated global residual norm defined in Eq. (25) is used as an indicator for termination criteria of the

adaptive process. The stopping criteria is defined as

$$\eta_g \leq \kappa_g \eta_{mg}, \tag{28}$$

where κ_g is the global residual tolerant and η_{mg} is the maximum global error indicator value throughout the adaptive process. Once the criteria is met, the adaptive process will be terminated.

5.3 Refinement procedure

The Delaunay diagram is used for locating the position of the additional nodes in the refinement process. Additional node will be inserted in the center of the Delaunay cell if the refinement criteria, Eq. (20), is met as shown in Fig. 4. As remeshing is not required at each adaptive step, the computation cost of the adaptive scheme is tremendously reduced compared to the weak-form method.

6 Numerical examples

A number of numerical examples is presented in this work. The following norm for true error is defined as

$$e = \sqrt{\frac{\sum (s^{\text{exact}} - s^{\text{appr}})^2}{\sum (s^{\text{exact}})^2}}, \tag{29}$$

where s^{exact} is the exact solution and s^{appr} numerical solution.

Example 1 The first example demonstrates the instability problem encountered by the RPCM. In this numerical example, a benchmark plane stress problem of solid mechanics is studied. A cantilever beam with unit thickness is subjected to a parabolic shear stress at the right

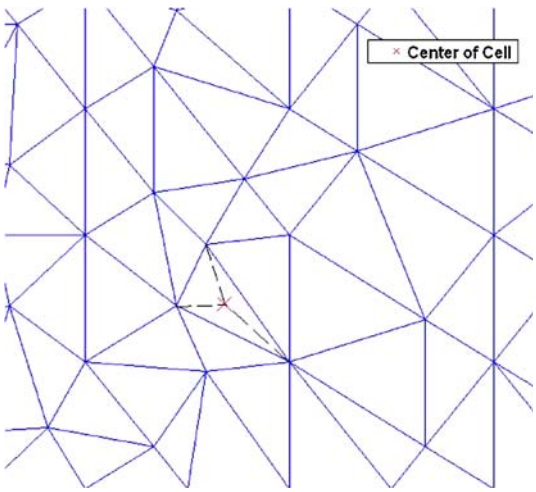

Fig. 4 Additional nodes inserted in the Delaunay cell

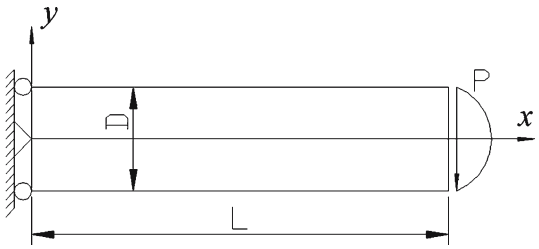

Fig. 5 Cantilever beam subjected to a parabolic shear stress at the *right* end

end as shown in Fig. 5. The material properties and geometrics are given as: Young's modulus $E = 3 \times 10^7$, Poisson's ratio $\upsilon = 0.3$, length of cantilever $L = 48.0\,\text{m}$ and the height $H = 12.0\,\text{m}$. The loading is known as $\tau_{xy} = -\frac{P}{2I}(H^2/4 - y^2)$, where I is moment of inertial of the cross section of cantilever and $P = 1{,}000\,\text{N}$.

The equilibrium equation has to be satisfied in the problem domain as

$$\sigma_{ij,j} + b_i = 0 \quad \text{in } \Omega. \tag{30}$$

Dirichlet boundary conditions are given as

$$u_i = \bar{u}_i \quad \text{on } \Gamma_u, \tag{31}$$

and Neumann boundary conditions are given as

$$\sigma_{ij} n_j = t_i \quad \text{on } \Gamma_t. \tag{32}$$

The analytical solution of this problem can be found in the [32].

From our study, the Neumann boundary condition is found as the cause of the instability. To demonstrate this argument, the cantilever is first modelled by 951 randomly distributed nodes in the problem domain. Another 12 nodes are added into the first model to make the second model with 963 nodes, that is the fact latter model is quite similar to the first model. As the analytical solution is known, the Dirichlet boundary condition is first imposed based on the analytical solution of displacements along all the boundaries. One can observe that the results of deflection along $x = 0$ m for both models are remained good and close to each other as shown in Fig. 6.

However, if the Dirichlet boundary condition is only imposed on the left edge and Neumann boundary conditions are imposed on the rest of the edges of the cantilever, the RPCM solutions of this problem for these two similar models are totally different as shown in Fig. 7. This example clearly reveals the inherited instability problem using conventional collocation method such as the RPCM. Therefore, an effective stabilization measure is a prerequisite for the RPCM before it is used in the adaptive analysis.

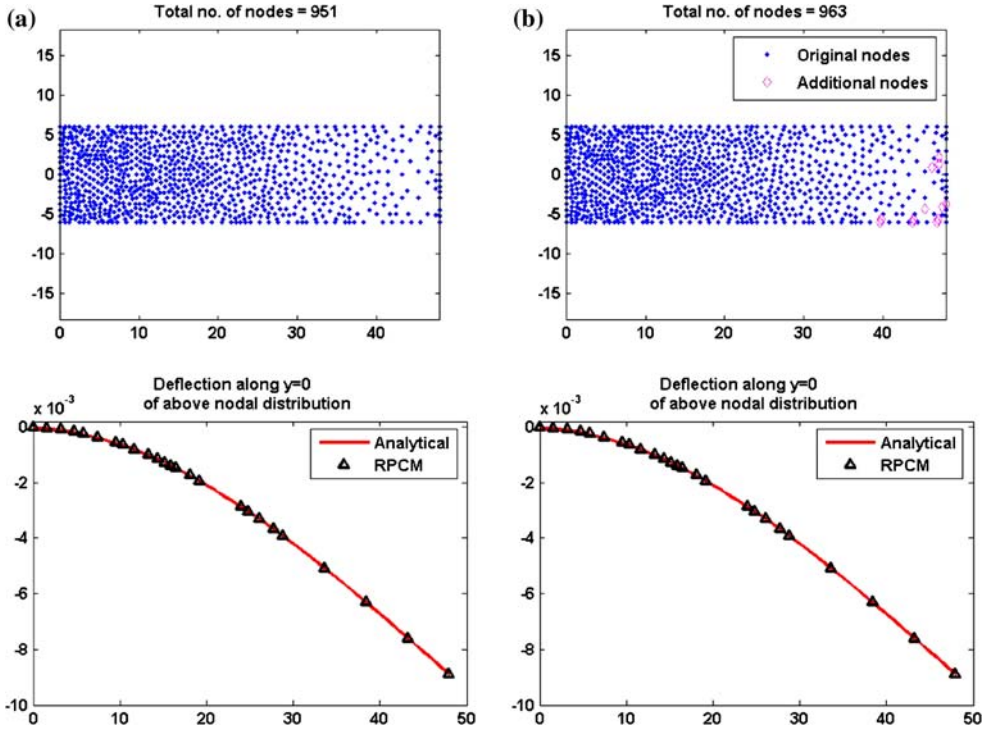

Fig. 6 Deflection of the cantilever beam for nodal distributions with **a** 951 nodes and **b** 963 nodes without Neumann boundary conditions

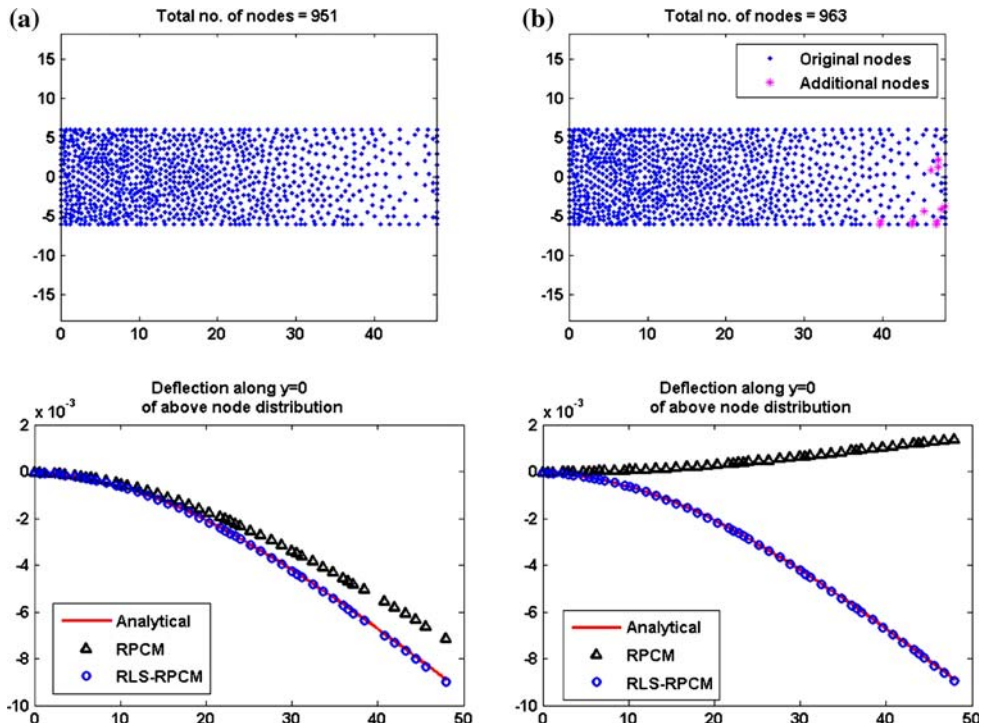

Fig. 7 Deflection of the cantilever beam for nodal distributions with **a** 951 nodes and **b** 963 nodes with Neumann boundary conditions

We had then used the regularization least-squares procedure described in Sect. 4 to stabilize the solution of the RPCM. The results for both models using the regularized least-squares RPCM (RLS-RPCM) are shown in Fig. 7. The solutions obtained by the RLS-RPCM with two models are good and close to each

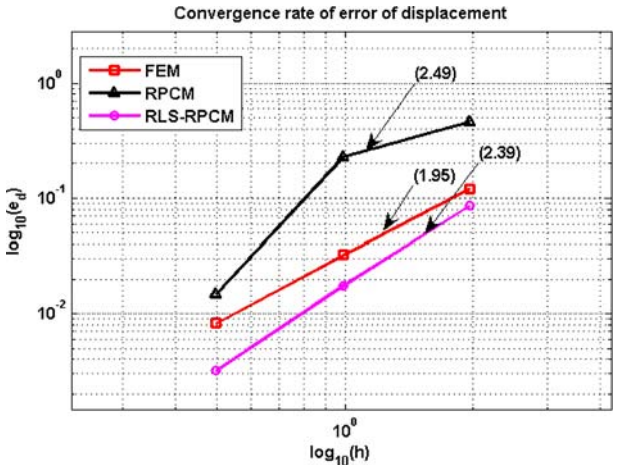

Fig. 8 Comparison of convergence rate among the FEM, RPCM and RLS-RPCM

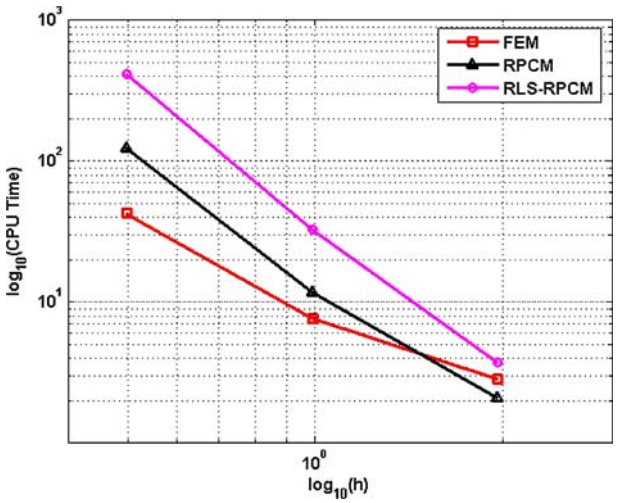

Fig. 9 Comparison of computational time among the FEM, RPCM and RLS-RPCM

other. The deflection of the cantilever obtained by the RLS-RPCM is also much closer to analytical solution compared to the RPCM.

To provide an overview of the computational cost and the accuracy of the RLS-RPCM, the solution of the RLS-RPCM is compared with the FEM and the RPCM. Four sets of regularly distributed nodes are used in this example, which are 25×7, 49×13 and 97×25 nodes. Linear triangular mesh is used in the FEM and nine nodes are used for the RPCM and the RLS-RPCM to construct their shape functions. The convergence rate and the computational time of three different numerical methods are shown in the Figs. 8 and 9. The convergence rate of FEM and RLS-RPCM is 1.95 and 2.39, respectively. One can found that the accuracy of the RLS-RPCM is comparable with the FEM. The accuracy of the solutions obtained by the RPCM for displacements

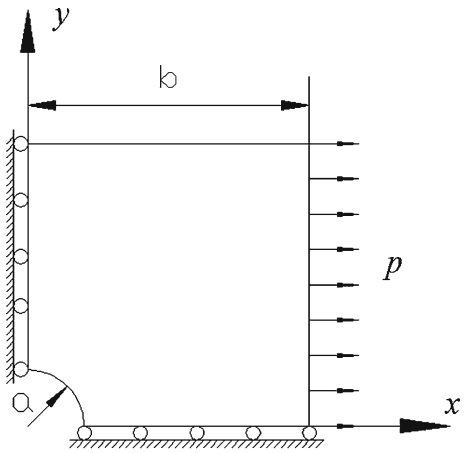

Fig. 10 Model of a plate subjected to an unit traction in the *horizontal* direction

is lower than other methods. However, the computational time of the RLS-RPCM is slightly higher that the RPCM.

Although the RLS-RPCM requires a little more computational time than the FEM, the RLS-RPCM possesses many attractive features to facilitate an easier implementation of adaptive analysis. No special technique is required in the refinement procedure and no remeshing is required at each adaptive step. A truly meshfree method not only avoid the mesh related problem but also facilitate a simple adaptive scheme.

It is also very important to note that the FEM only ensures that the displacement is continuous over the entire problem domain. To provide a better approximation for stresses, post-processing treatment is required for the FEM. In contrast, the RLS-RPCM provides a convenience to obtain both displacements and stresses in the entire problem domain.

Example 2 The second numerical example is an adaptive analysis of an infinite plate with circular hole subjected to an unit traction P in the horizontal direction. A plane strain case is considered in this example. Due to the symmetry, only quarter of the problem is modelled as shown in Fig. 10. The geometry and material properties are given as: $a = 0.2$, $b = 2.0$, Young's modules $E = 1 \times 10^3$ and Poisson's ratio $\upsilon = 0.3$.

The governing equations for this problem are same as Example 1 and given as Eqs. (30)–(32). Symmetric boundary conditions are imposed on the left and right edges. Analytical solutions can be found in [32].

The adaptive analysis started with 121 nodes irregularly distributed in the problem domain. Twelve nodes are used in support domain for constructing the shape function. The local refinement coefficient is predefined as $\kappa_l = 0.1$ and the global residual tolerant is set as

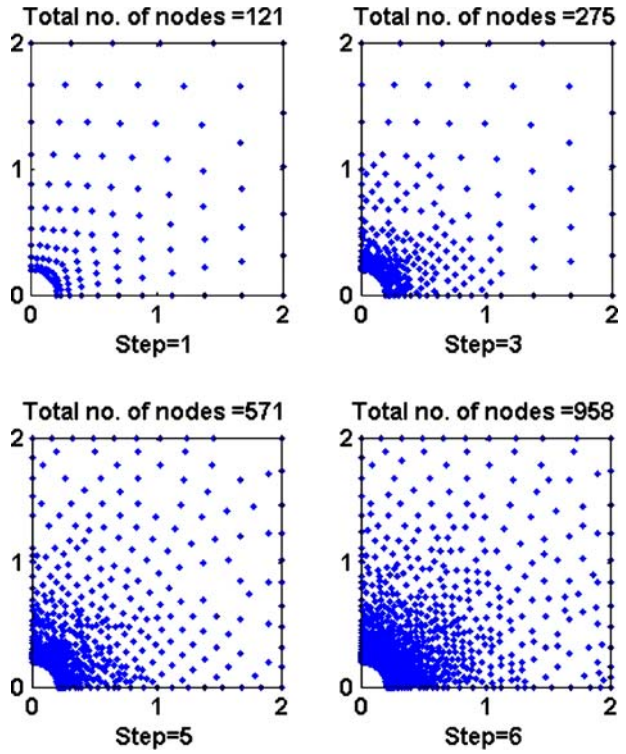

Fig. 11 Nodal distributions at 1st, 3rd, 5th and 6th step

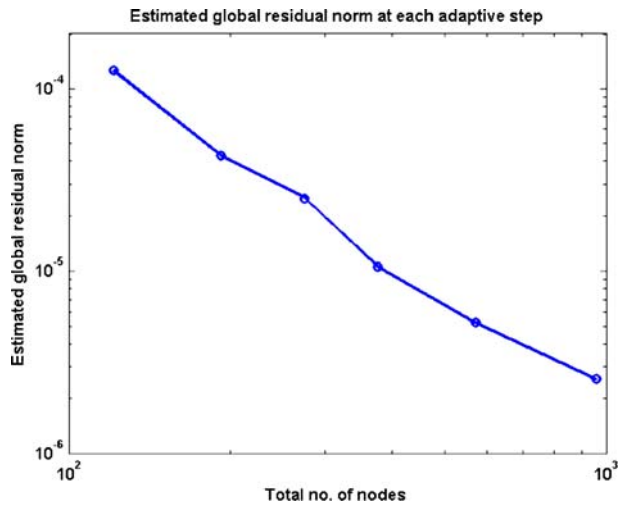

Fig. 12 Estimated global residual norm at each adaptive step for Example 2

$\kappa_g = 0.025$. The adaptive analysis ended at 6th step with 958 nodes irregularly distributed in the problem domain, as shown in Fig. 11.

The estimated global residual norm at each adaptive step is plotted in Fig. 12. One can notice that the estimated global residual norm is gradually reduced at each adaptive step, it demonstrates excellent stability of the RSL-RPCM. The error norm of the displacements in

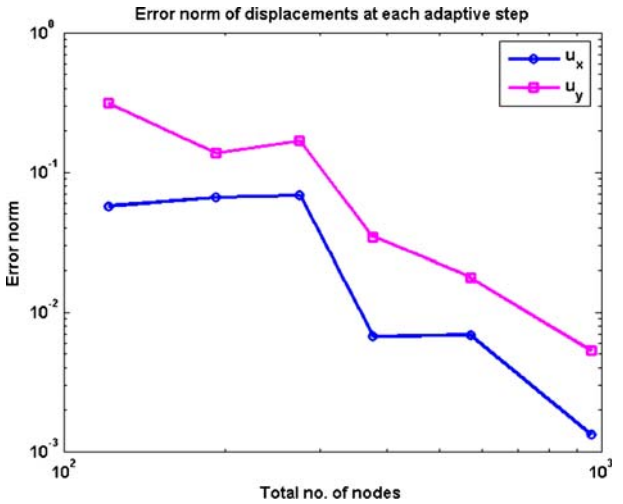

Fig. 13 Error norms of displacements at each adaptive step for Example 2

x and y direction are also plotted in Fig. 13. The error norms have been dramatically reduced from initial step 5.7 and 31.32% to 0.13 and 0.53% at last step.

For reference purpose, the displacements in y direction along the left edge and displacements in x direction along bottom edge are plotted at initial and final steps as shown in Fig. 14 . The normal stresses and shear stresses along the left edge at initial and final steps are also shown in Fig. 15. It is evidently clear that the accuracy of both displacements and stresses have been greatly improved thru the effective adaptive scheme.

Example 3 In this example, an adaptive analysis for a bridge with irregular geometry is studied. A half model of the bridge is studied due to its symmetric, and a plane strain problem is considered. A constant pressure $P = 1{,}000$ N/m^2 is subject to the top of the bridge. The dimension of the bridge is shown in Fig. 16 and the material properties are given as: Young's modulus $E = 4 \times 10^9$ and Poisson's ratio $\upsilon = 0.15$.

This example is first started with 246 nodes in the problem domain as shown in Fig. 17. Only 12 nodes are used for the local function approximation. The local refinement coefficient is preset as $\kappa_l = 0.1$ and the global residual tolerant is predefined as $\kappa_g = 0.1$. The adaptive process is terminated at the 8th step with 1,118 nodes as shown in Fig. 17.

The estimated global residual norm at each adaptive step is given in the Fig. 18. As no analytical solution is available in this case, reference solutions for displacements and stresses are obtained using ANSYS with very fine quadrilateral mesh. The displacements in y direction along the left edge and top edge of the bridge are plotted in Fig. 19. The solutions obtained by the RLS-RPCM through the adaptive analysis are in very good

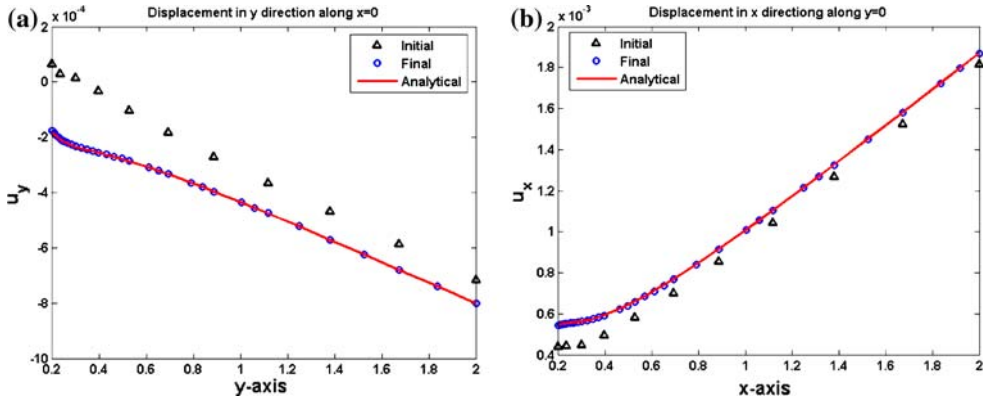

Fig. 14 Displacements **a** u_y along the $x = 0$, and **b** u_x along the $y = 0$ at initial and final steps

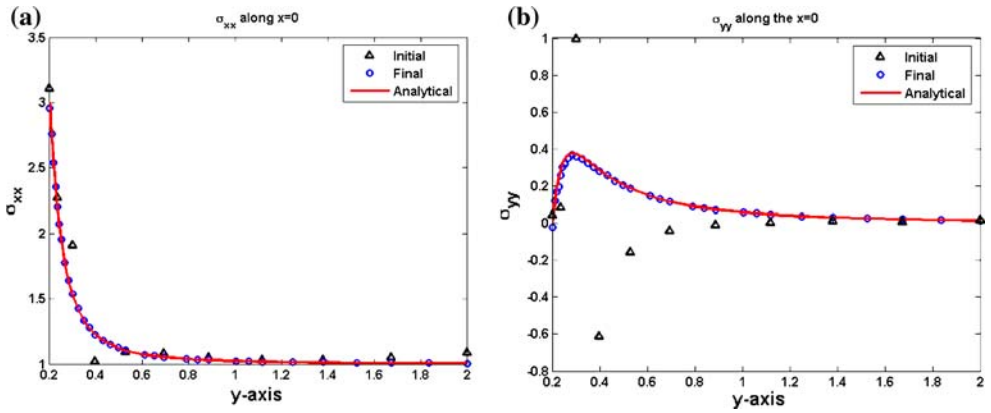

Fig. 15 Normal stresses **a** σ_{xx} and **b** τ_{xy} along the $x = 0$ at initial and final steps

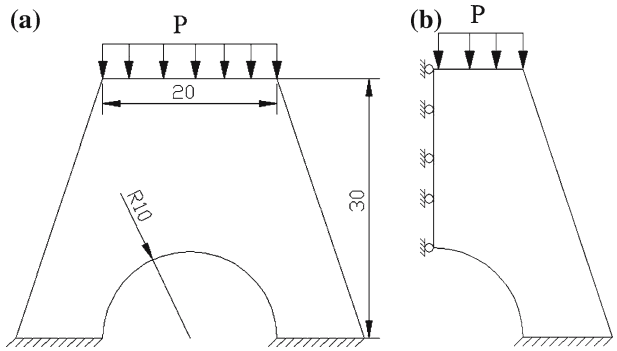

Fig. 16 A bridge subjected to a constant pressure on *top* with **a** full model and **b** a half model

agreement with the references solutions. Besides the displacements, the normal stresses σ_{xx} and σ_{yy} along the left edge are also plotted in Fig. 20. The stresses obtained by the RLS-RPCM through adaptive analysis are also in very good agreement with the reference solutions.

Example 4 In example 4, an adaptive analysis for Poisson problem whose solution has sharp peak is studied. Considered a Poisson equation is defined as

$$\nabla^2 u = \left[-400 + (200x - 100)^2 + (200y - 100)^2\right] \cdot \mathrm{e}^{-100\left(x-\frac{1}{2}\right)^2 - 100\left(y-\frac{1}{2}\right)^2}, \tag{33}$$

in domain of $\Omega : [0,1] \times [0,1]$, with Neumann boundary conditions,

$$\frac{\partial u}{\partial n} = 0 \quad \text{along } \Gamma_t : x = 0 \text{ and } y = 0, \tag{34}$$

and with Dirichlet boundary conditions,

$$u = 0 \quad \text{along } \Gamma_t : x = 1 \text{ and } y = 1. \tag{35}$$

The analytical solution for this problem is given as

$$u = \mathrm{e}^{-100\left(x-\frac{1}{2}\right)^2 - 100\left(y-\frac{1}{2}\right)^2}. \tag{36}$$

The plots for the exact solutions of the field function u and its derivatives are given in the Fig. 21.

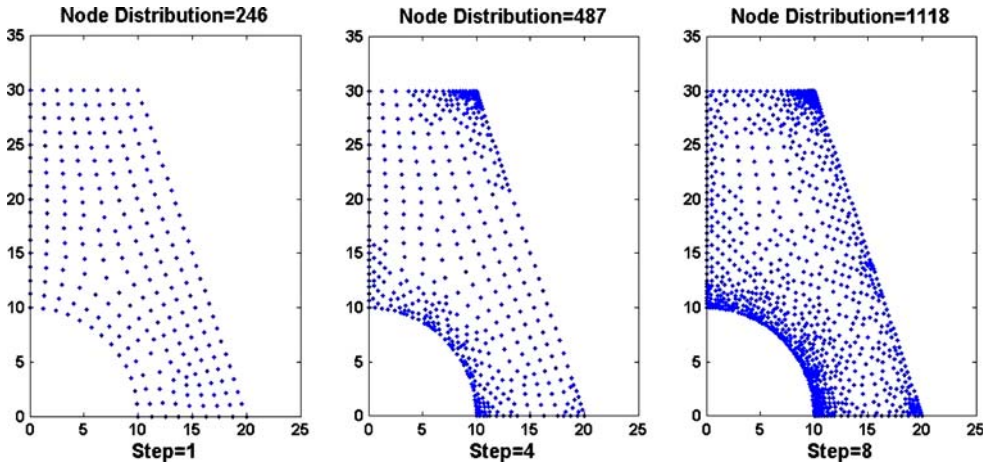

Fig. 17 A bridge subjected to a constant pressure on *top*

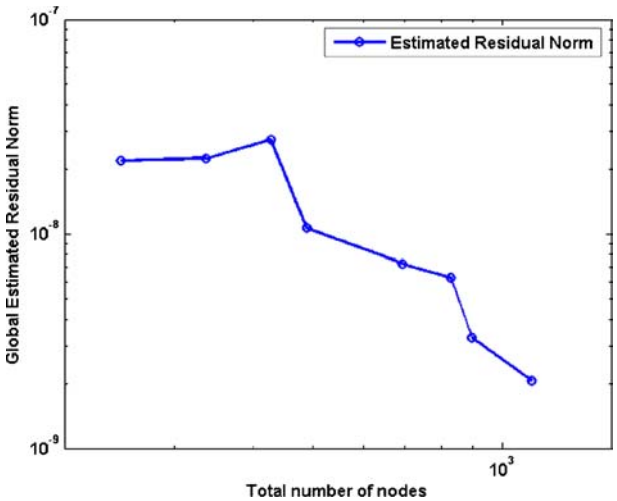

Fig. 18 Estimated global residual norm at each adaptive step for Example 3

The Poisson problem is first started with 100 regularly distributed nodes and ended up at 8th step with 8,337 nodes in the problem domain. The local refinement coefficient is predefined as $\kappa_l = 0.1$ and the global residual tolerant is predefined as $\kappa_g = 0.1$. Due to the presence of high peak, most of the nodes are inserted at the high gradient region as shown in Fig. 22. From Fig. 23, one can observe that the estimated global residual norm is reduced gradually. While estimated global residual norm is reduced in the adaptive process, the error norm of the field function is also gradually reduced from 29.76 to 0.32% as shown in Fig. 24.

The approximated values of field function u along $y = 0.5$ at initial and final steps are plotted with analytical solution as shown in Fig. 25. It is evidently clear that proposed adaptive scheme is effective to improve the accuracy of the solution for field function u. A three dimensional plot of approximated field function and its derivatives at the final step is also provided in the Fig. 26. It shows not only that the approximated field function but also the approximated field function derivatives are in very good agreement with analytical solutions shown in the Fig. 21.

Example 5 In this example, another Poisson problem whose solution has multiple peaks is considered. The purpose of this example is to show the robustness of the simple error indicator for multi peak solution in a problem domain. The Poisson equation is considered as follows:

$$\nabla^2 u = 2\pi^2(\cos 2\pi x \sin^2 2\pi y + \cos 2\pi y \sin^2 2\pi x) \qquad (37)$$

in the domain $\Omega : [-1,1] \times [-1,1]$, with Neumann boundary conditions

$$\frac{\partial u}{\partial n} = 0 \quad \text{along } \Gamma_t : x = 1;\ y = 1, \qquad (38)$$

and with Dirichlet boundary conditions

$$u = 0 \quad \text{along } \Gamma_u : x = -1;\ y = -1. \qquad (39)$$

The exact solution of field function u is known as

$$u = \sin^2 \pi x \sin^2 \pi y \qquad (40)$$

The three dimensional plot of the exact solution is plotted in the Fig. 27, four peaks can be observed in problem domain.

In this example, ten nodes are used for the local function approximation. The local refinement coefficient is predefined as $\kappa_l = 0.1$ and global residual tolerant value is predefined as $\kappa_g = 0.01$. The adaptive analysis started with 100 regularly distributed nodes and ended at 12th step with 10,764 nodes. As there are four peaks exist

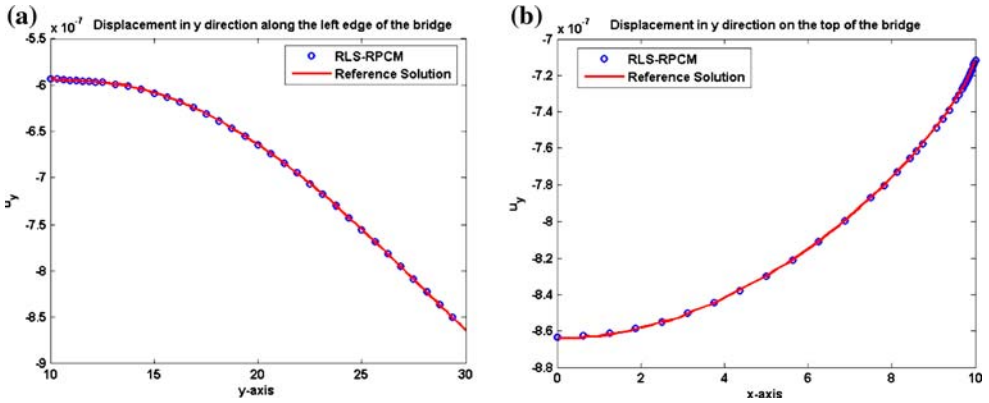

Fig. 19 Displacements in y direction along the **a** *left* edge and **b** *top* of the bridge

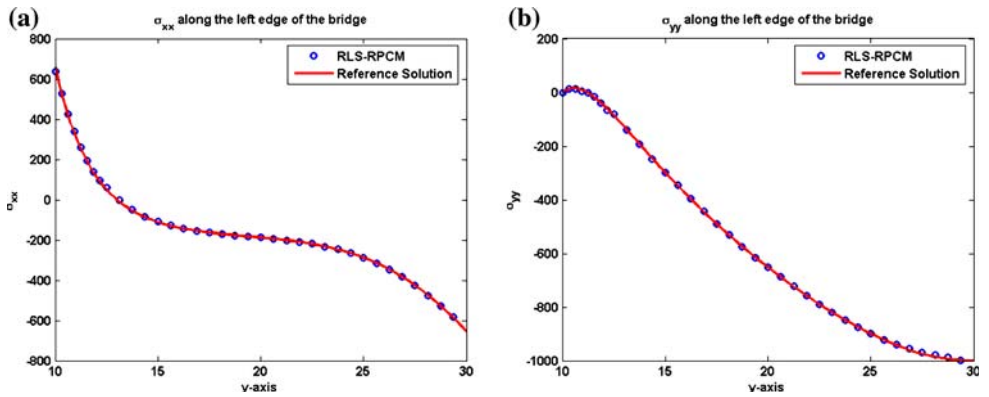

Fig. 20 The normal stresses **a** σ_{xx} and **b** σ_{yy} along the *left* edge of the bridge

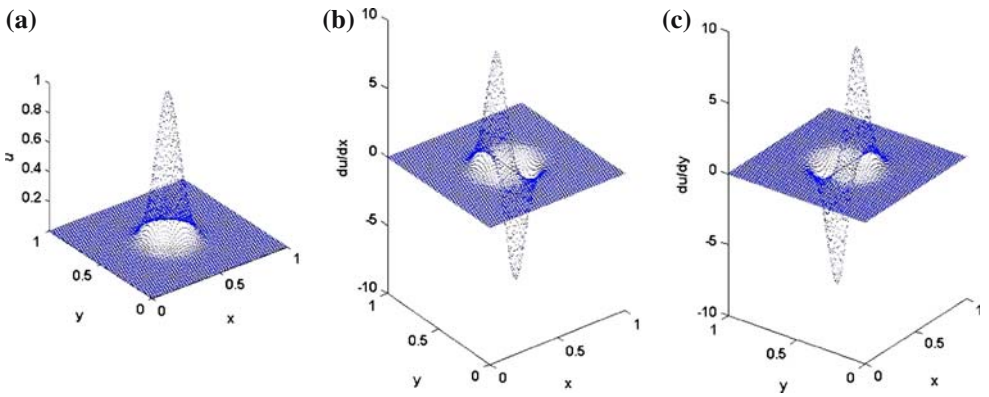

Fig. 21 Three dimensional plots for **a** field function u, **b** $\frac{\partial u}{\partial x}$ and **c** $\frac{\partial u}{\partial y}$

in the problem domain, one can observe four rings of dense node distributions are appeared at the final step, as shown in Fig. 28.

For strong-form adaptive method, the accuracy of the solution at the stage of refinement is very much relying on the current node distribution. In this work, our error estimation is based on residual in the strong formulation, and no variational principle is used. Therefore, one can observe that the global residual norm is monotonically reduced rather than the error of the field function (as shown in Figs. 29, 30). This is true that if there is sufficient number of nodes to the capture the peaks. Nevertheless,

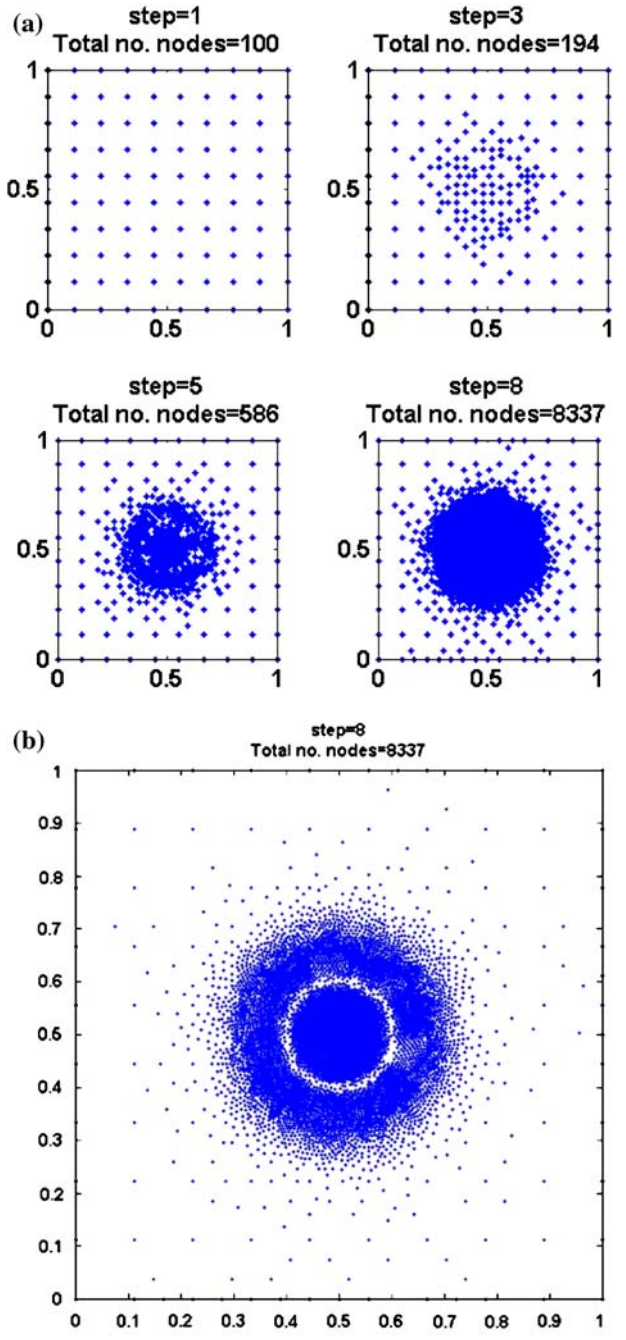

Fig. 22 **a** The nodal distribution at 1st, 3rd, 5th and 8th steps, and **b** an enlarged view of the node distribution at the final step

the overall error of the field function has been gradually reduced in the overall adaptive process. From Fig. 30, one can observe that the error norm of the field variable is dramatically reduced from 324 to 0.62% in 12 steps. The field function values u along the $y = 0.5$ at first, fourth and final step are also plotted in the Fig. 31. The accuracy of the solution for u is improved through the adaptive scheme.

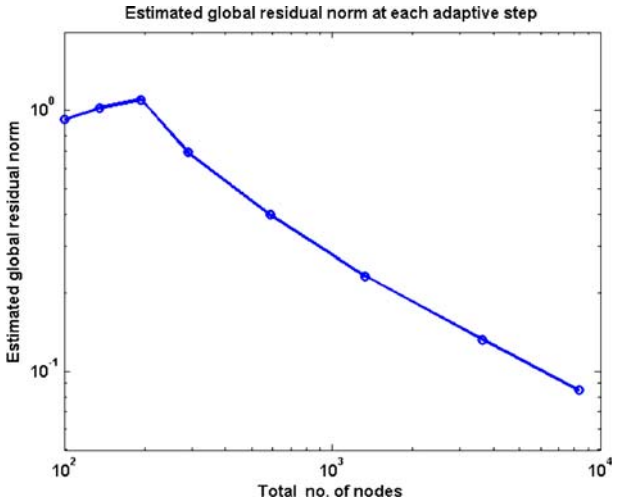

Fig. 23 Estimated residual norm at each adaptive step for Example 4

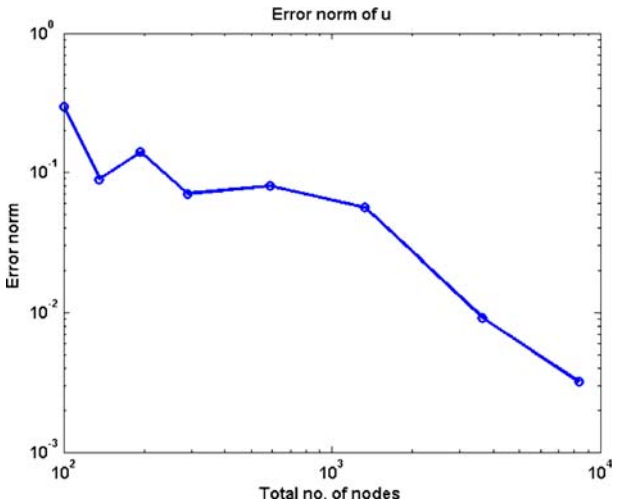

Fig. 24 Error norm of field function u at each adaptive step for Example 4

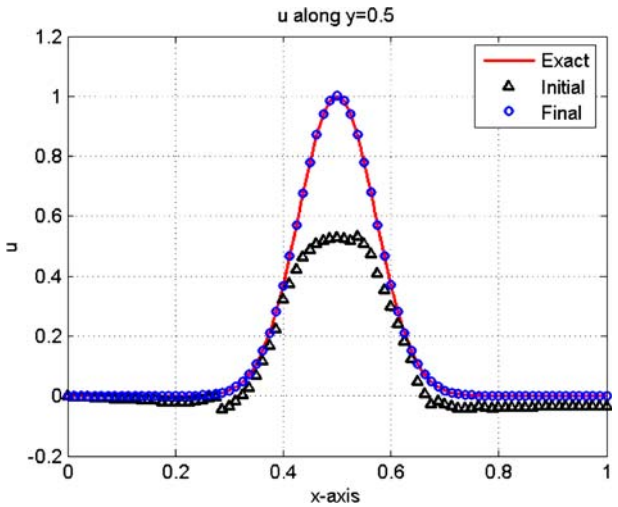

Fig. 25 Approximated values of field function u along $y = 0.5$ at first and final steps

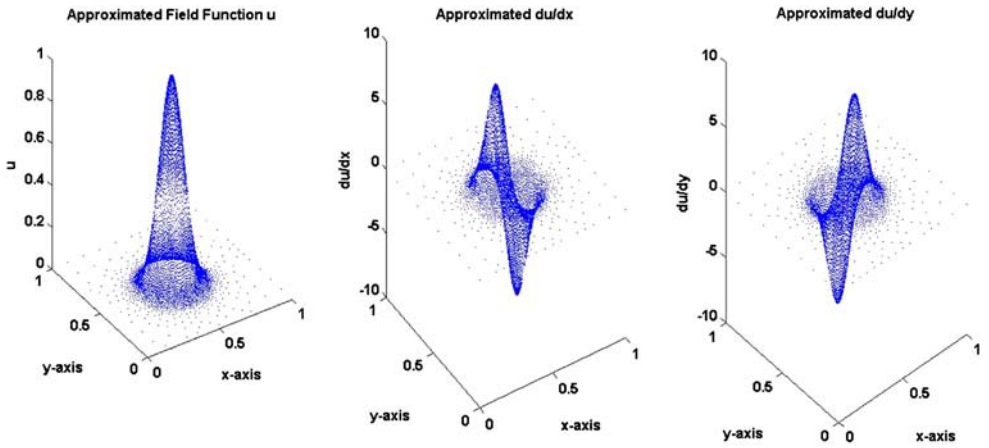

Fig. 26 The three dimensional plots for field function u and its derivatives at the final adaptive step

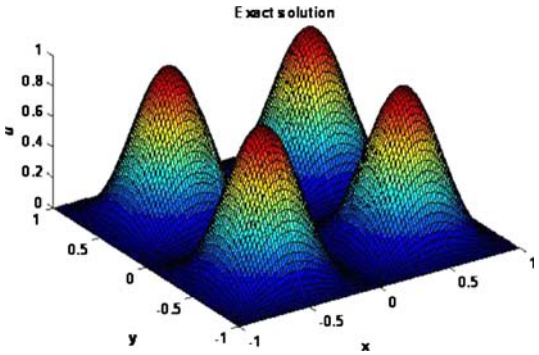

Fig. 27 Exact solution of the field function u

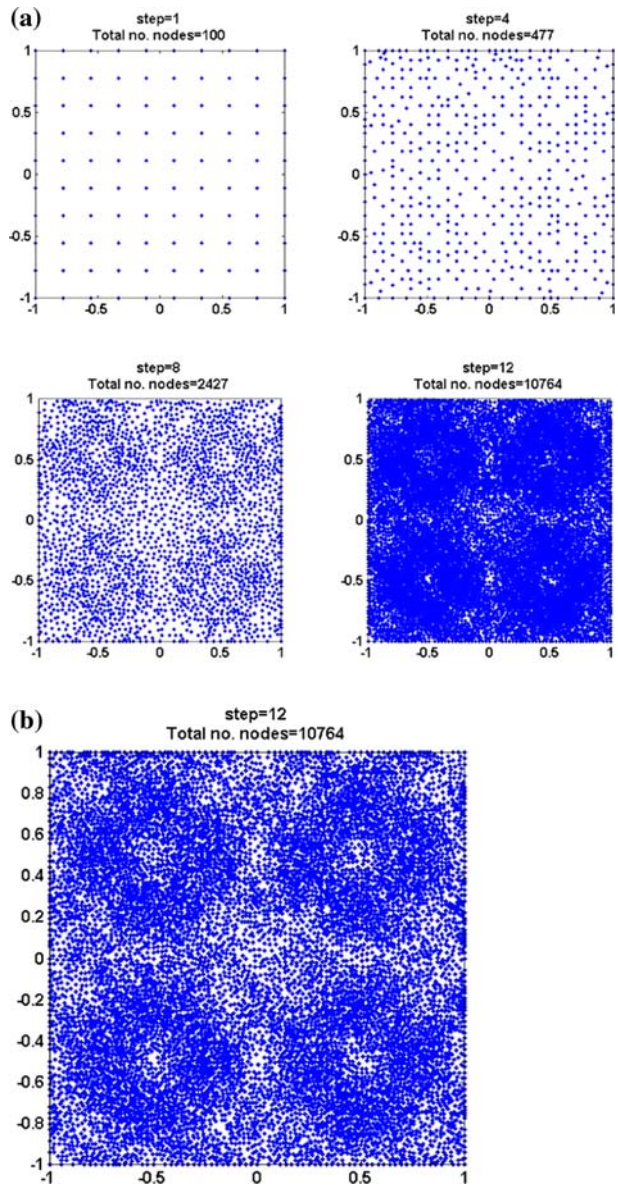

Fig. 28 **a** The nodal distributions at 1st, 4th, 8th, and 12th step, and **b** the enlarged view of the nodal distribution of the final step

7 Concluding remarks

In this paper, a novel stabilized meshfree strong-form method is proposed. Regularization technique which often used for the ill-posed inversed problems has successfully stabilised the solution of RPCM for the forward problems. From the numbers of numerical problems in this works, stable and accurate results are shown by the RLS-RPCM. As the stability is ensured, the features of the meshfree strong-form methods can therefore be utilized to facilitate an easier implementation of adaptive analysis. As the RLS-RPCM is a truly meshfree method, the expensive computation cost of remeshing process can be avoided. Simple refinement scheme using Delaunay diagram can be used without undue worry of nodal connectivity. In this work, an effective error estimator based on residual is also introduced. The residual based error estimator is simple and yet effectively reflects the quality of local approximation and the global accuracy of the solution. The accuracy of the solution has been improved in the adaptive analysis as shown in the numerical examples.

However, the RLS-RPCM requires slightly higher computational cost compared to the RPCM. The small

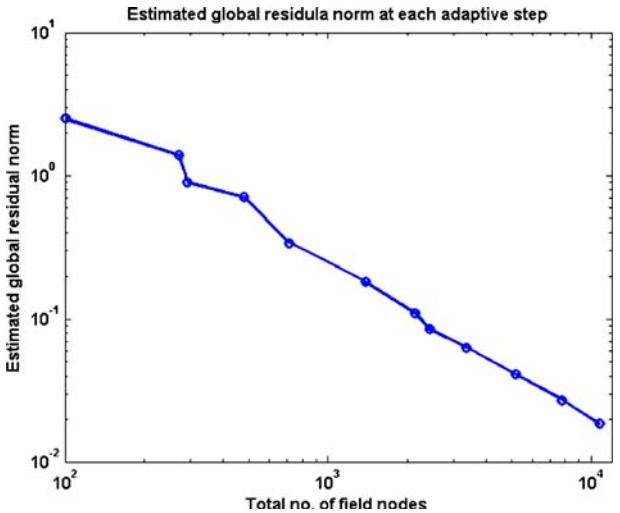

Fig. 29 Estimated global residual norm at each adaptive step for Example 5

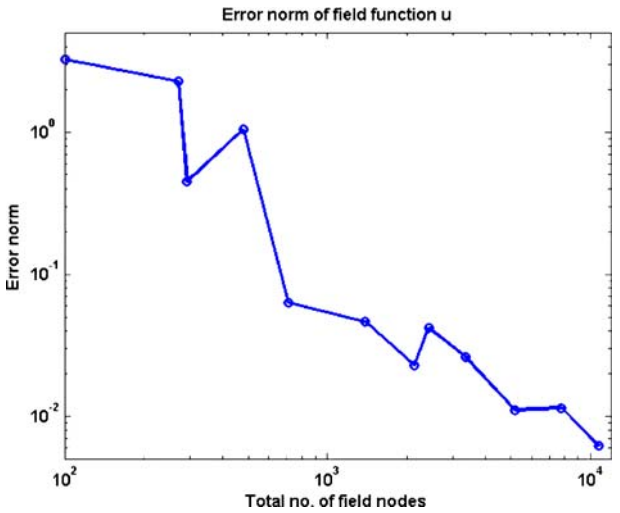

Fig. 30 Exact error norm of field function u at each adaptive step for Example 5

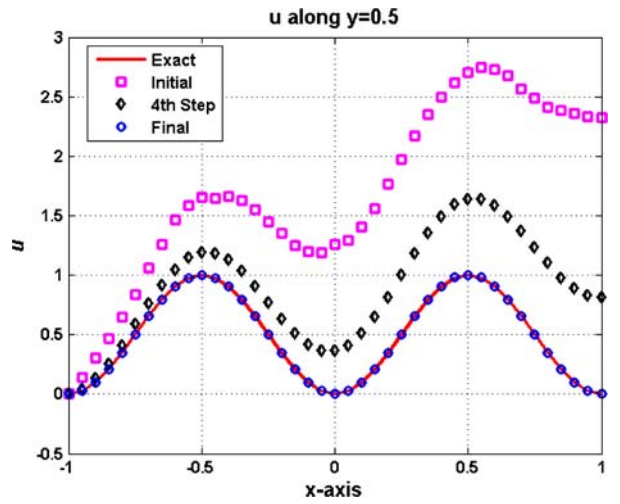

Fig. 31 Field function values u along $y = 0.5$ at first, fourth and final steps

additional cost introduced by the regularization procedure is to acquire the crucial stability and accuracy in the solution. Nevertheless, this small amount of additional cost is usually insignificant in the adaptive analysis.

The development of meshfree strong-form method is still very sluggish compared to weak-form method. The stability is still remained the most challenging issue in the strong-form method. This paper provides a possible approach to restore the stability and successfully implemented the stabilized strong-from method for the adaptive analysis. There is still a big room for the improvement. At the current stage, this RLS-RPCM is only restricted for linear problem. It can be extended for more complex problem such as nonlinear and dynamics problem. The RLS-RPCM is also not considered for the incompressible material at this stage.

References

1. Atluri SN, Zhu T (1998) A new meshless local Petrov-Galerkin (MLPG) approach in computational mechanics. Comput Mech 22:117–127
2. Belytschko T, Lu YY, Gu L (1994) Element-free Galerkin method. Int J Numer Methods Eng 37:229–256
3. Belytschko T, et al (1996) Meshfree method: an overview and recent development. Comput Methods Appl Eng 139:229–256
4. Franke R (1982) Scattered data interpolation: test of some methods. Math Comput 38(157):181–200
5. Franke C, Schaback R (1998) Solving partial differential equations by collocation using radial basis functions. Appl Math Comput 93:73–82
6. Golberg MA, Chen CS, Karur SR (1996) Improved multiquadrics approximation for partial differential equations. Eng Anal Bound Elem 18:9–17
7. Hansen PC (1992) Analysis of discrete ill-posed problems by means of the L-curve. SIAM Rev 34:561–580
8. Hardy RL (1990) Theory and applications of multiquadrics-Biharmonic method (20 years of discovery 1968–1988). Comput Math Appl 19(8/9):163–208
9. Hon YC, Lu MW, Xue WM, Zhu YM (1997) Multiquadric method for the numerical solution of a biphasic mixture model. Appl Math Comput 88:153–175
10. Jun S, Liu WK, Belytschko T (1998) Explicit reproducing kernel particle methods for large deformation problem. Int J Numer Methods Eng 41:137–166
11. Kansa EJ (1990) Multiquadrics—a scattered data approximation scheme with applications to computational fluid-dynamics I and II. Comput Math Appl 19(8/9):127–161
12. Kansa EJ, Hon YC (2000) Circumventing the ill-conditioning problem with multiquadric radial basis functions: application to elliptic partial differential equations. Comput Math Appl 39:123–137
13. Li Y, Liu GR, Luan MT, Dai KK, Zhong ZH, Li GY, Han X (2006) Contact analysis for solids based on linearly conforming RPIM. Comput Mech (in press)
14. Liu GR (2002) Meshfree method: moving beyond the finite element method. CRC Press, Boca Raton, Florida
15. Liu GR, Gu YT (2001) A point interpolation method for two-dimensional solids. Int J Numer Methods Eng 50:937–951

16. Liu GR, Gu YT (2001) A local radial point interpolation method (LRPIM) for free vibration analyses of 2-D solids. J Sound Vib 246:29–46
17. Liu GR, Gu YT (2003) A meshfree method: meshfree weak-strong form method for 2-D solids. Comput Mech 33:2–14
18. Liu GR, Gu YT (2005) An introduction to meshfree methods and their programming. Springer, Berlin Heidelberg New York
19. Liu GR, Han X (2003) Computational inverse techniques in non-destructive evaluation. CRC Press, Boca Raton, Florida
20. Liu WK, Jun S (1998) Multiple scale reproducing kernel particle methods for large deformation problems. Int J Numer Methods Eng 41:1339–1362
21. Liu GR, Kee BBT (2005) An adaptive meshfree method based on regularized least-squares formulation. In: 13th International conference on computational and experimental engineering and sciences (ICCES), Chennai, India
22. Liu GR, Liu MB (2003) Smoothed particle hydrodynamics: a meshfree particle method. World Scientific, New Jersey
23. Liu GR, Wu YL, Ding H (2004) Meshfree weak-strong (MWS) form method and its application to incompressible flow problems. Int J Numer Methods Fluids 46:1025–1047
24. Liu GR, Zhang GY, Gu YT, Wang YY (2005) A meshfree radial point interpolation method (RPIM) for three-dimensional solids. Comput Mech 36:421–430
25. Liu GR, Zhang GY, Dai KY (2005) A linear conforming point interpolation method (LC-PIM) for 2D solid mechanics problems. Int J Comput Methods 2(4):645–665
26. Liu X, Liu GR, Tai K, Lam KY (2005) Radial basis interpolation collocation method for the solution of partial differential equations. Comput Math Appl 50:1425–1442
27. Monaghan JJ (1988) An introduction to SPH. Comput Phys Commum 48:89–96
28. Nayroles B, Touzot G, Villon P (1992) Generalizing the finite element method: diffuse approximation and diffuse elements. Comput Mech 10:307–318
29. Onãte E, Perazzo F, Miquel J (2001) A finite point method for elasticity problems. Comput Struct 79:2153–2163
30. Power H, Barraco V (2002) A comparison analysis between unsymmetric and symmetric radial basis function collocation methods for the numerical solution of partial differential equations. Comput Math Appl 43(3–5):551–583
31. Tikhonov AN, Stepanov AV, Yagola AG (1990) Numerical methods for the solutions of ill-posed problems. Kluwer, Dordrecht
32. Timoshenko SP, Goodier JN (1970) Theory of elasticity. McGraw-Hill, New York
33. Wang JG, Liu GR (2002) On the optimal shape parameters of radial bais bfunctions. Comput Methods Appl Mech Eng 191:21–26
34. Wang JG, Liu GR (2002) A point interpolation meshless methods based on radial basis functions. Int Numer Methods Eng 54:1623–1648
35. Zhang X, Song KZ, Lu MW, Liu X (2001) Meshless methods based on collocation with radial basis functions. Comput Mech 26(1):29–46